Analysis and Design of Numerical Schemes for Gas Dynamics 2 Artificial Diffusion and Discrete Shock Structure

Antony Jameson
Department of Mechanical and Aerospace Engineering
Princeton University
Princeton, New Jersey 08544 USA

Abstract

The effect of artificial diffusion on discrete shock structures is examined for a family of schemes which includes scalar diffusion, convective upwind and split pressure (CUSP) schemes, and upwind schemes with characteristic splitting. The analysis leads to conditions on the diffusive flux such that stationary discrete shocks can contain a single interior point. The simplest formulation which meets these conditions is a CUSP scheme in which the coefficients of the pressure differences is fully determined by the coefficient of convective diffusion. It is also shown how both the characteristic and CUSP schemes can be modified to preserve constant stagnation enthalpy in steady flow, leading to four variants, the E and H-characteristic schemes, and the E and H-CUSP schemes. Numerical results are presented which confirm the properties of these schemes.

1 Introduction

The development of computational methods for the solution of gas dynamic equations has presented a continuing challenge. The goal of combining

1. high accuracy
2. high resolution of shock waves and contact discontinuities without oscillation
3. minimum computational complexity

in a single scheme has proved elusive. Two main issues in the design of non-oscillatory high resolution schemes were identified in the previous paper of this series [9]; first the design of scalar discrete schemes which guarantee the preservation of positivity and monotonicity in the solution, and second the construction of numerical fluxes for systems of equations to allow the proper resolution of complex wave interactions which may lead to the formation of both shock waves and contact discontinuities. The earlier paper develops systematic procedures for the design of scalar discretization schemes which satisfy positivity constraints. The present paper focuses on the design of numerical fluxes for the gas dynamic equations.

Results presented in the previous paper confirm that stationary shocks can be resolved with a single interior point by combining either a symmetric limited positive (SLIP) scheme or an upstream limited positive (USLIP) scheme with a characteristic decomposition of the diffusive flux. The present paper presents an analysis of the conditions under which a discrete stationary shock can contain a single interior point. It emerges that a characteristic decomposition is not necessary to meet these conditions. Perfect single point discrete shocks completely free of oscillations can be produced by simpler flux splittings belonging to the class of convective

upwind and split pressure (CUSP) schemes, in which scalar diffusion is augmented by pressure differences. It is actually possible to obtain high resolution with almost no oscillation by introducing the right amount of of scalar diffusion, though this seems to result in a scheme which is less robust than the CUSP scheme.

Section 2 reviews the shock jump conditions for one-dimensional flow, and their relationship to Roe's linearization [15]. Section 3 reviews alternative splittings for a family of schemes. In all of them the diffusive flux is defined by a matrix which can be expressed as a polynomial function of the Jacobian matrix. Section 4 examines semi-discrete schemes for the one-dimensional gas dynamic equations, and analyzes the conditions under which the numerical fluxes can be in perfect equilibrium when the discrete shock structure contains one interior point. These constraints can be satisfied by any numerical flux such that the equilibrium across the interface at the exit of the shock corresponds to the Hugoniot equation for a moving shock, while equilibrium across the interface at the entrance to the shock is maintained by full upwinding. The Roe linearization can be used to construct a variety of fluxes with these properties, with or without characteristic decomposition. In steady-state calculations the total enthalpy should be constant. Unfortunately numerical fluxes derived from the standard characteristic decomposition are not compatible with this property. Section 5 shows how the splittings can be modified so that this property is recovered while the discrete shock structure still has a single interior point. Section 6 discusses the implementation of limiters for these schemes. Numerical results which confirm the properties of the schemes are presented in section 7.

2 Shock Jump Conditions and Roe Linearization

The general one dimensional conservation law for a system of equations can be expressed as

$$\frac{\partial w}{\partial t} + \frac{\partial}{\partial x} f(w) = 0. \tag{1}$$

For the equations of gas dynamics the state and the flux vectors are

$$w = \begin{pmatrix} \rho \\ \rho u \\ \rho E \end{pmatrix}, \quad f = \begin{pmatrix} \rho u \\ \rho u^2 + p \\ \rho u H \end{pmatrix},$$

where ρ is the density, u is the velocity, E is the total energy, p is the pressure, and H is the stagnation enthalpy. If γ is the ratio of specific heats and c is the speed of sound then

$$p = (\gamma - 1)\rho \left(E - \frac{u^2}{2} \right)$$
$$c^2 = \frac{\gamma p}{\rho}$$
$$H = E + \frac{p}{\rho} = \frac{c^2}{\gamma - 1} + \frac{u^2}{2}.$$

In a steady flow H is constant. This remains true for the discrete scheme only if the numerical diffusion is constructed so that it is compatible with this condition.

When the flow is smooth it can be represented by the quasi-linear form

$$\frac{\partial w}{\partial t} + A(w)\frac{\partial w}{\partial x} = 0,$$

where $A(w) = \frac{\partial f}{\partial w}$, and the eigenvalues u, $u + c$ and $u - c$ of the Jacobian matrix A are the wave speeds for the three characteristics. In smooth flow the entropy S is constant along streamlines, and in isentropic flow the Riemann invariants $R^{\pm} = u \pm \frac{2c}{\gamma - 1}$ are constant along the characteristics $\frac{dx}{dt} = u \pm c$. These conditions may be expressed by the three equations,

$$\frac{\partial R^+}{\partial t} + (u + c)\frac{\partial R^+}{\partial x} \quad = \quad 0$$

$$\begin{aligned} \frac{\partial R^-}{\partial t} + (u-c)\frac{\partial R^-}{\partial x} &= 0 \\ \frac{\partial S}{\partial t} + u\frac{\partial S}{\partial x} &= 0. \end{aligned}$$

Taking the dependent variables as

$$w = \begin{pmatrix} \frac{2c}{\gamma-1} \\ u \\ S \end{pmatrix},$$

the equations can be expressed in the symmetric form

$$\frac{\partial \tilde{w}}{\partial t} + \tilde{A}(\tilde{w})\frac{\partial \tilde{w}}{\partial x} = 0,$$

where

$$\tilde{A}(\tilde{w}) = \begin{pmatrix} u & c & 0 \\ c & u & 0 \\ 0 & 0 & u \end{pmatrix}.$$

Depending on the initial data, there may not be a smooth solution of the conservation law (1). Nonlinear wave interactions along converging characteristics may lead to the formation and propagation of shock waves, while contact discontinuities may also appear. Denote the left and right states across a shock by subscripts L and R, and let $[f]$ and $[w]$ be the jumps $f_R - f_L$ and $w_R - w_L$. The shock jump condition is then

$$[f] = \mathcal{S}\,[w]\,,$$

where $\mathcal{S}$ is the shock speed.

In order to simplify the analysis of the equations when there are finite jumps in w and f, Roe introduced the linearization

$$f_R - f_L = A_{RL}(w_R, w_L)(w_R - w_L).$$

where $A_{RL}(w_R, w_L)$ is a Jacobian matrix calculated from the left and right states in such a way that this relation is exact [15]. He showed that one way to do this is to introduce weighted averages

$$u = \frac{\sqrt{\rho_R}u_R + \sqrt{\rho_L}u_L}{\sqrt{\rho_R} + \sqrt{\rho_L}}, \quad H = \frac{\sqrt{\rho_R}H_R + \sqrt{\rho_L}H_L}{\sqrt{\rho_R} + \sqrt{\rho_L}} \tag{2}$$

into all the formulas in the standard expression for the Jacobian matrix $A(w)$. In the case of a shock wave it now follows that

$$A_{RL}(w_R - w_L) = \mathcal{S}(w_R - w_L).$$

Thus the shock speed $\mathcal{S}$ is an eigenvalue of A_{RL}, and the jump $w_R - w_L$ is an eigenvector. In the case of a stationary shock $S = 0$. If we consider flow with $u > 0$ only the eigenvalue $u - c$ can be zero. It follows that when u and c are calculated with Roe averages, $u = c$ for a stationary shock.

3 Alternative Splittings

Suppose that the conservation law (1) is approximated over the interval $(0, L)$ on a mesh with an interval Δx by the semi-discrete scheme

$$\Delta x \frac{dw_j}{dt} + h_{j+\frac{1}{2}} - h_{j-\frac{1}{2}} = 0, \tag{3}$$

where w_j denotes the value of the discrete solution in cell j, and $h_{j+\frac{1}{2}}$ is the numerical flux between cells j and $j+1$. Let f_j denote the flux vector $f(w_j)$ evaluated for the state w_j. Suppose also that the numerical flux is

$$h_{j+\frac{1}{2}} = \frac{1}{2}(f_{j+1} + f_j) - d_{j+\frac{1}{2}}, \tag{4}$$

where $d_{j+\frac{1}{2}}$ is a diffusive flux which is introduced to enable the scheme to resolve discontinuities without producing oscillations in the discrete solution. The diffusive flux is assumed to have the form

$$d_{j+\frac{1}{2}} = \frac{1}{2}\alpha_{j+\frac{1}{2}} B_{j+\frac{1}{2}}(w_{j+1} - w_j),$$

where the matrix $B_{j+\frac{1}{2}}$ determines the properties of the scheme, and the scaling factor $\alpha_{j+\frac{1}{2}}$ is included for convenience. Introducing a Roe linearization, let $A_{j+\frac{1}{2}}(w_{j+1}, w_j)$ be an estimate of the Jacobian matrix $\frac{\partial f}{\partial w}$ with the property that

$$A_{j+\frac{1}{2}}(w_{j+1} - w_j) = f_{j+1} - f_j. \tag{5}$$

$A_{j+\frac{1}{2}}$ can be decomposed as

$$A_{j+\frac{1}{2}} = T\Lambda T^{-1},$$

where the columns of T are the eigenvectors of $A_{j+\frac{1}{2}}$, and Λ is a diagonal matrix containing its eigenvalues. Then the upwind scheme is produced by setting

$$B_{j+\frac{1}{2}} = \left|A_{j+\frac{1}{2}}\right| = T\left|\Lambda\right| T^{-1}, \tag{6}$$

where the notation $\left|A_{j+\frac{1}{2}}\right|$ is used to represent the absolute value of $A_{j+\frac{1}{2}}$ which is defined to be the matrix obtained by replacing the eigenvalues by their absolute values. Scalar diffusion is produced by setting

$$B_{j+\frac{1}{2}} = I. \tag{7}$$

An intermediate class of schemes can be formulated by defining the first order diffusive flux as a combination of differences of the state and flux vectors

$$d_{j+\frac{1}{2}} = \alpha_{j+\frac{1}{2}}\left(w_{j+1} - w_j\right) + \beta_{j+\frac{1}{2}}\left(f_{j+1} - f_j\right).$$

Schemes of this class are fully upwind in supersonic flow if one takes $\alpha_{j+\frac{1}{2}} = 0$ and $\beta_{j+\frac{1}{2}} = \text{sign}(M)$ when the absolute value of the Mach number M exceeds 1. The flux vector f can be decomposed as

$$f = uw + f_p, \tag{8}$$

where

$$f_p = \begin{pmatrix} 0 \\ p \\ up \end{pmatrix}. \tag{9}$$

Then

$$f_{j+1} - f_j = \bar{u}\left(w_{j+1} - w_j\right) + \bar{w}\left(u_{j+1} - u_j\right) + f_{p_{j+1}} - f_{p_j}, \tag{10}$$

where $\bar{u}$ and $\bar{w}$ are the arithmetic averages

$$\bar{u} = \frac{1}{2}\left(u_{j+1} + u_j\right), \quad \bar{w} = \frac{1}{2}\left(w_{j+1} + w_j\right).$$

All these schemes can be obtained by representing $B_{j+\frac{1}{2}}$ as a polynomial in the matrix $A_{j+\frac{1}{2}}$ defined by equation (5). Schemes using polynomial expnasions of the Jacobian matrix have also been considered by Van Leer [10]. According to the Cayley-Hamilton theorem, a matrix satisfies its own characteristic equation. Therefore the third and higher powers of A can be eliminated, and there is no loss of generality in limiting $B_{j+\frac{1}{2}}$ to a polynomial of degree 2,

$$B_{j+\frac{1}{2}} = \alpha_0 I + \alpha_1 A_{j+\frac{1}{2}} + \alpha_2 A^2_{j+\frac{1}{2}}. \tag{11}$$

The characteristic upwind scheme for which $B_{j+\frac{1}{2}} = \left|A_{j+\frac{1}{2}}\right|$ is obtained by substituting $A_{j+\frac{1}{2}} = T\Lambda T^{-1}$, $A^2_{j+\frac{1}{2}} = T\Lambda^2 T^{-1}$. Then α_0, α_1, and α_2 are determined from the three equations

$$\alpha_0 + \alpha_1\lambda_k + \alpha_2\lambda_k^2 = \left|\lambda_k\right|, \quad k = 1, 2, 3.$$

The same representation remains valid for three-dimensional flow because $A_{j+\frac{1}{2}}$ still has only three distinct eigenvalues u, $u+c$, $u-c$.

Since $w_{j+1} - w_j$ approximates $\Delta x \frac{\partial w}{\partial x}$, the diffusive flux introduces an error proportional to the mesh width, and both these schemes will be first order accurate unless compensating anti-diffusive terms are introduced.

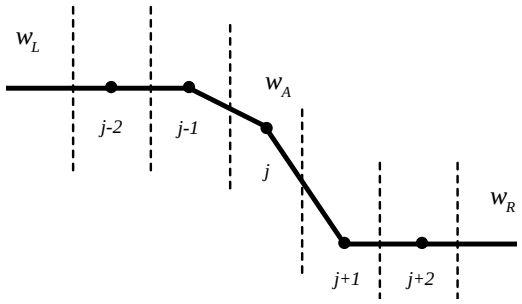

Figure 1: Shock structure for single interior point.

4 Conditions for a Stationary Shock

The model of a discrete shock which will be examined is illustrated in figure (1). Suppose that w_L and w_R are left and right states which satisfy the jump conditions for a stationary shock, and that the corresponding fluxes are $f_L = f(w_L)$ and $f_R = f(w_R)$. Since the shock is stationary $f_L = f_R$. The ideal discrete shock has constant states w_L to the left and w_R to the right, and a single point with an intermediate value w_A. The intermediate value is needed to allow the discrete solution to correspond to a true solution in which the shock wave does not coincide with an interface between two mesh cells. According to equation (1)

$$\int_0^L w(T)dx = \int_0^L w(0)dx - \int_0^T (f_{RB} - f_{LB})dt,$$

where f_{LB} and f_{RB} are the fluxes at the left and right boundaries. Assuming that the boundary conditions are compatible with a steady solution containing a stationary shock, the location x_s of the shock is fixed by this equation, since

$$\int_0^L w(T)dx = x_s w_L + (L - x_s)w_R.$$

Similarly in the semi-discrete system

$$\Delta x \sum_j w_j(T) = \Delta x \sum_j w_j(0) - \int_0^T (f_{RB} - f_{LB})dt. \tag{12}$$

Thus $\sum_j w_j(T)$ has a value which is determined by the initial and boundary conditions, and in general it is not possible for this value to be attained by a discrete solution without an intermediate point, because then the sum would be quantized, increasing by $\Delta x(w_R - w_L)$ whenever the shock location is shifted one cell to the right.

Three diffusion models of varying complexity are examined in the following paragraphs to determine their ability to support the ideal shock structure containing a single interior point. These correspond to one, two or three terms in equation (11). A discrete shock structure with a finite number of interior points has the advantage that it could be contained in an otherwise smooth solution without contaminating the accuracy of the smooth parts. In a one-dimensional flow such a structure allows discrete solutions in exact agreement with the true solution outside the shock region.

4.1 Case 1 Scalar Diffusion

The first model is simple scalar diffusion with

$$d_{j+\frac{1}{2}} = \frac{1}{2}\alpha_{j+\frac{1}{2}}(w_{j+1} - w_j).$$

Consider the equilibrium in the cell immediately to the right of the shock. Using subscripts AR and RR to denote the values at the cell boundaries, the outgoing flux is

$$h_{RR} = \frac{1}{2}(f_R + f_R) - \frac{1}{2}\alpha_{RR}(w_R - w_R) = f_R,$$

while the incoming flux is

$$h_{AR} = \frac{1}{2}(f_R + f_A) - \frac{1}{2}\alpha_{AR}(w_R - w_A).$$

For equilibrium these must be equal. It follows that

$$f_R - f_A + \alpha_{AR}(w_R - w_A) = 0.$$

This is the Hugoniot condition for a shock moving to the left with a speed α_{AR}. Introduce a Roe linearization with a mean Jacobian matrix $A_{AR}(w_A, w_R)$ such that

$$f_R - f_A = A_{AR}(w_R - w_A).$$

Then $w_R - w_A$ is an eigenvector of A_{AR} corresponding to the eigenvalue $-\alpha_{AR}$. The eigenvalues of A_{AR} are u, $u + c$ and $u - c$. If we consider flow to the right with $u > 0$, and $u < c$, a solution with positive numerical diffusion is obtained by taking $\alpha_{AR} = |u - c|$. Then the intermediate value w_A must lie on a Hugoniot curve defined by the right state w_R.

When the corresponding equilibrium is considered for a cell immediately to the left of a shock wave in a flow moving to the left, it is found that the diffusion coefficient should be $|u + c|$. Both cases can be satisfied by taking $\alpha = \min(|u + c|, |u - c|)$. In the neighborhood of a stagnation point the accuracy can be improved by taking α proportional to u to prevent the numerical diffusion becoming undesirably large. This suggests the strategy of using a diffusion coefficient proportional to the smallest eigenvalue, or

$$\alpha_{j+\frac{1}{2}} = \min_k |\lambda_k|,$$

where λ_k are the eigenvalues u, $u + c$, and $u - c$ of $A_{j+\frac{1}{2}}$. To prevent the scheme from admitting stationary expansion shocks which would violate the entropy condition, the diffusion coefficient may be redefined as

$$\alpha_{j+\frac{1}{2}} = \min_k \hat{\lambda}_k, \tag{13}$$

where

$$\hat{\lambda}_k = \begin{cases} |\lambda_k| & \text{if } |\lambda_k| \geq \lambda_0 \\ \frac{1}{2}(\lambda_0 + \frac{|\lambda_k|^2}{\lambda_0}) & \text{if } |\lambda_k| < \lambda_0, \end{cases} \tag{14}$$

and λ_0 is a positive threshold proportional to c. Recent work of Aiso [1] has established that in the scalar case this modification of the viscosity is sufficient to guarantee that the discrete solution will satisfy the entropy condition. The usual strategy in schemes using scalar diffusion has been to make the diffusion coefficient proportional to the maximum eigenvalue of the Jacobian matrix $\frac{\partial f}{\partial w}$, in order to make sure that the numerical viscosity for each characteristic variable is large enough to satisfy the positivity condition. Numerical tests with the alternative strategy of using the smallest eigenvalue confirm that very sharp discrete shocks are obtained, and that the scheme is robust with a viscosity threshold of the type defined by equation (14).

To determine whether scalar diffusion can exactly support an ideal discrete shock it is also necessary to examine the equilibrium in the cell immediately before the shock. In this case the numerical fluxes are

$$h_{LL} = f_L,$$

and

$$h_{LA} = \frac{1}{2}(f_A + f_L) - \frac{1}{2}\alpha_{LA}(w_A - w_L).$$

For equilibrium it is necessary that

$$f_A - f_L - \alpha_{LA}(w_A - w_L) = 0,$$

which is the Hugoniot condition for a shock moving to the right with a speed α_{LA}. Introducing the Roe linearization, $w_A - w_L$ must now be an eigenvector of A_{LA}. The transition from L to A, however, is less than the full jump for a stationary shock for which it is known that Roe averaging results in $u = c$. Thus it may be expected that $u > c$, and the choice $\alpha_{LA} = u - c = |u - c|$ could still allow the equilibrium condition to be satisfied. Then w_A lies on a Hugoniot curve defined by the left state w_L.

The question now arises whether an intermediate state w_A can be found that simultaneously lies on Hugoniot curves defined by the left and right states w_L and w_R, where these two states themselves satisfy the Hugoniot condition for a steady shock. It turns out that this is not possible. Let $v = \frac{1}{\rho}$ be the specific volume. Then all possible shocks connecting w_L and w_R must satisfy the Hugoniot relation

$$p_R v_R - p_L v_L = \frac{\gamma - 1}{2}(p_R + p_L)(v_L - v_R). \tag{15}$$

This establishes a locus on a $p - v$ diagram of a family of shocks as the shock speed is varied. The single point shock structure requires w_A to lie on the Hugoniot curves defined by w_L and w_R. The curve defined from w_L is

$$p_A v_A - p_L v_L = \frac{\gamma - 1}{2}(p_A + p_L)(v_L - v_A), \tag{16}$$

while the curve from w_R is

$$p_R v_R - p_A v_A = \frac{\gamma - 1}{2}(p_R + p_A)(v_A - v_R). \tag{17}$$

These intersect only when $w_A = w_R$ or w_L. To prove this note that (15) can be written as

$$p_R v_R - p_L v_L = \alpha(p_R v_L - p_L v_R), \tag{18}$$

where $\alpha = \frac{\gamma-1}{\gamma+1}$. Similarly (16) and (17) yield

$$p_A = p_L \frac{v_L - \alpha v_A}{v_A - \alpha v_L} = p_R \frac{v_R - \alpha v_A}{v_A - \alpha v_R}.$$

Thus v_A satisfies a quadratic equation which may be written as

$$(p_R v_R - p_L v_L)v_A - \alpha(p_R - p_L)(v_A^2 + v_L v_R) + \alpha^2 v_A(p_R v_L - p_L v_R) = 0.$$

Substituting from equation (18)

$$v_A(p_R v_L - p_L v_R) - (p_R - p_L)(v_A^2 + v_L v_R) + v_A(p_R v_R - p_L v_L) = 0,$$

or

$$(p_R - p_L)(v_A - v_R)(v_A - v_L) = 0.$$

If $p_L \neq p_R$ this has only the solutions $v_A = v_L$ or $v_A = v_R$. Therefore it is concluded that scalar diffusion cannot support a perfect discrete shock with a single interior point. Calculations of one-dimensional flows reveal an oscillation of very small amplitude upstream of the shock. In multidimensional flows, however, these oscillations are essentially imperceptible.

4.2 Case 2 Characteristic Upwind Scheme

The second case to be examined is the upwind scheme which results from characteristic decomposition, with $B_{j+\frac{1}{2}} = \left|A_{j+\frac{1}{2}}\right|$. This case has been studied by Roe [16], and it is known that the upwind scheme admits ideal shocks. Assuming flow to the right with $u > 0$, the fluxes in the cell to the right of the shock are now

$$h_{RR} = f_R,$$

and

$$h_{AR} = \frac{1}{2}(f_R + f_A) - \frac{1}{2}\left|A_{AR}\right|(w_R - w_A),$$

yielding equilibrium if

$$(A_{AR} - |A_{AR}|)(w_R - w_A) = T(\Lambda - |\Lambda|)T^{-1}(w_R - w_A) = 0.$$

With $u < c$ this is satisfied by the negative eigenvalue $u-c$, and since $w_R - w_A$ is the corresponding eigenvector, the Hugoniot equation

$$f_R - f_A = S(w_R - w_A)$$

is satisfied for the shock speed $S = u - c$. Thus w_A again lies on a Hugoniot curve. At the entrance to the shock the transition from w_L to w_A is less than the full transition from w_L to w_R for which $u = c$. Thus a structure is admitted in which $u > c$ in the transition from L to A, with the consequence that the flux is calculated from the upwind state

$$h_{LA} = \frac{1}{2}(f_A + f_L) - \frac{1}{2}A_{LA}(w_L - w_A) = f_L$$

and equilibrium is maintained.

4.3 Case 3 Convective Upwind and Split Pressure (CUSP) Scheme

Characteristic decomposition allows equilibrium to be established through full upwinding of the flux entering the transition layer, while the flux leaving the transition layer satisfies a Hugoniot equation. This can also be accomplished by a less complex scheme. Suppose that the diffusive flux is defined as

$$d_{j+\frac{1}{2}} = \frac{1}{2}\alpha^* c(w_{j+1} - w_j) + \frac{1}{2}\beta(f_{j+1} - f_j),$$

where the factor c is included so that α^* is dimensionless. Let M be the Mach number $\frac{u}{c}$. If the flow is supersonic an upwind scheme is obtained by setting

$$\alpha^* = 0, \;\; \beta = \text{sign}(M).$$

Introducing the Roe linearization, the Mach number is calculated from u and c, and at the entrance to the shock a transition to an intermediate value w_A is admitted with $u > c$ and

$$h_{LA} = \frac{1}{2}(f_A + f_L) - \frac{1}{2}(f_A - f_L) = f_L.$$

The fluxes leaving and entering the cell immediately to the right of the shock are now

$$h_{RR} = f_R,$$

and

$$h_{AR} = \frac{1}{2}(f_R + f_A) - \frac{1}{2}\alpha^* c(w_R - w_A) - \frac{1}{2}\beta(f_R - f_A).$$

These are in equilibrium if

$$f_R - f_A + \frac{\alpha^* c}{1+\beta}(w_R - w_A) = 0.$$

This is the Hugoniot equation for a shock moving to the left with a speed $\frac{\alpha^* c}{1+\beta}$. Also, introducing the Roe linearization,

$$(A_{AR} + \frac{\alpha^* c}{1+\beta} I)(w_R - w_A) = 0.$$

Thus $w_R - w_A$ is an eigenvector of A_{AR} and $-\frac{\alpha^* c}{1+\beta}$ is the corresponding eigenvalue. Since the eigenvalues are u, $u+c$ and $u-c$, the only choice which leads to positive diffusion when $u > 0$ is $u-c$, yielding the relationship

$$\alpha^* c = (1+\beta)(c-u), \ 0 < u < c.$$

Thus β is uniquely determined once α^* is chosen, leading to a one-parameter family of schemes. The choice $\beta = M$ corresponds to the Harten-Lax-Van Leer (HLL) scheme [5, 3], which is extremely diffusive.

The term $\beta(f_R - f_A)$ contributes to the diffusion of the convective terms. Suppose that the convective terms are separated by splitting the flux according to equations (8), (9) and (10). Then the total effective coefficient of convective diffusion is

$$\alpha c = \alpha^* c + \beta \bar{u}.$$

The choice $\alpha c = \bar{u}$ leads to low diffusion near a stagnation point, and also leads to a smooth continuation of convective diffusion across the sonic line since $\alpha^* = 0$ and $\beta = 1$ when $|M| > 1$. The scheme must also be formulated so that the cases of $u > 0$ and $u < 0$ are treated symmetrically. Using the notation $M = \frac{u}{c}$, $\lambda^{\pm} = u \pm c$, this leads to the diffusion coefficients

$$\alpha = |M| \tag{19}$$

$$\beta = \begin{cases} +\max\left(0, \frac{u+\lambda^-}{u-\lambda^-}\right) & \text{if } 0 \le M \le 1 \\ -\max\left(0, \frac{u+\lambda^+}{u-\lambda^+}\right) & \text{if } -1 \le M \le 0 \\ \text{sign}(M) & \text{if } |M| \ge 1. \end{cases} \tag{20}$$

Near a stagnation point α may be modified to $\alpha = \frac{1}{2}\left(\alpha_0 + \frac{|M|^2}{\alpha_0}\right)$ if $|M|$ is smaller than a threshold α_0. The expression for β in subsonic flow can also be expressed as

$$\beta = \begin{cases} \max(0, 2M-1) & \text{if } 0 \le M \le 1 \\ \min(0, 2M+1) & \text{if } -1 \le M \le 0 \end{cases}$$

Equation (20) remains valid when the CUSP scheme is modified as described below in Section 5.2 to allow solutions with constant stagnation enthalpy. The coefficients $\alpha(M)$ and $\beta(M)$ are displayed in figure 2 for the case when $\alpha_0 = 0$. The cutoff of β when $|M| < \frac{1}{2}$, together with α approaching zero as $|M|$ approaches zero,

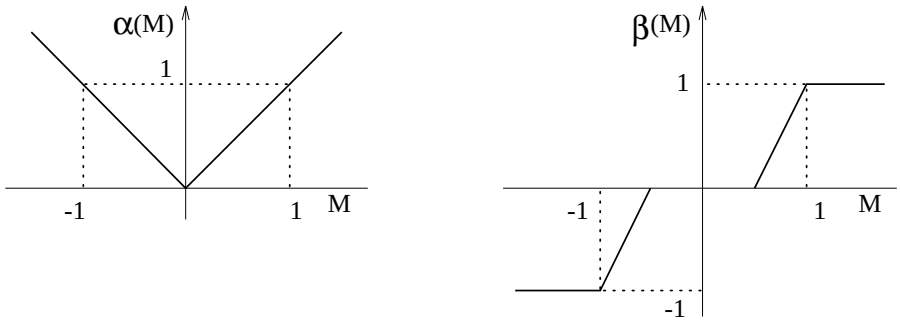

Figure 2: Diffusion Coefficients.

is also appropriate for the capture of contact discontiuities.

4.3.1 Criteria for a single point stationary shock

The analysis of these three cases shows that a discrete shock structure with a single interior point is supported by artificial diffusion that satisfies the two conditions that

1. it produces an upwind flux if the flow is determined to be supersonic through the interface
2. it satisfies a generalized eigenvalue problem for the exit from the shock of the form

$$(A_{AR} + \alpha_{AR} B_{AR})\,(w_R - w_A) = 0,$$

where A_{AR} is the linearized Jacobian matrix and B_{AR} is the matrix defining the diffusion for the interface AR. These two conditions are satisfied by both the characteristic and CUSP schemes. Scalar diffusion does not satisfy the first condition.

In an unsteady flow a single point shock structure could be instantaneously supported by a semi-discrete scheme with fluxes satisfying the same conditions. Then $h_{LA} = f_L$ and $h_{AR} = f_R$, with the consequence that the rate of change of the integrated state in the intermediate cell is

$$\Delta x \frac{dw_A}{dt} = f_R - f_L = s(w_R - w_L)$$

This is consistent with the motion of the shock wave across the cell. With a discrete time stepping scheme, however, such a structure cannot in general persist, because only a particular choice of the time step would bring w_A to w_L during one time step. On the other hand it is necessary to use a fixed time step throughout the mesh, and if the scheme is explicit, the time step must also be restricted to assure stability.

5 Schemes Admitting Constant Total Enthalpy in Steady Flow

In steady flow the stagnation enthalpy H is constant, corresponding to the fact that the energy and mass equations are consistent when the constant factor H is removed from the energy equation. Discrete and semi-discrete schemes do not necessarily satisfy this property. In the case of a semi-discrete scheme expressed in viscosity form, equations (3) and (4), a solution with constant H is admitted if the viscosity for the energy equation reduces to the viscosity for the continuity equation with ρ replaced by ρH. When the standard characteristic decomposition (6) is used, the viscous fluxes for ρ and ρH which result from composition of the fluxes for the characteristic variables do not have this property, and H is not constant in the discrete solution. In practice there is an excursion of H in the discrete shock structure which represents a local heat source. In very high speed flows the corresponding error in the temperature may lead to a wrong prediction of associated effects such as chemical reactions.

The source of the error in the stagnation enthalpy is the discrepancy between the convective terms

$$u \begin{pmatrix} \rho \\ \rho u \\ \rho H \end{pmatrix},$$

in the flux vector, which contain ρH, and the state vector which contains ρE. This may be remedied by introducing a modified state vector

$$w_h = \begin{pmatrix} \rho \\ \rho u \\ \rho H \end{pmatrix}.$$

Isenthalpic formulations have been considered by Veuillot and Viviand [19], and Lytton [13].

One may now introduce the linearization

$$f_R - f_L = A_h (w_{h_R} - w_{h_L}).$$

Here A_h may be calculated in the same way as the standard Roe linearization. On introducing the vector

$$v = \begin{pmatrix} \sqrt{\rho} \\ \sqrt{\rho}u \\ \sqrt{\rho}H \end{pmatrix},$$

all quantities in both f and w_h are products of the form $v_j v_k$ which have the property that a finite difference $\Delta(v_j v_k)$ between left and right states can be expressed as

$$\Delta(v_j v_k) = \bar{v_j}\Delta v_k + \bar{v_k}\Delta v_j$$

where $\bar{v_j}$ is the arithmetic mean $\frac{1}{2}(v_{jR} + v_{jL})$. Therefore,

$$\Delta w = B\Delta v, \;\; \Delta f = C\Delta v = CB^{-1}\Delta w,$$

where B and C can be expressed in terms of appropriate mean values of the quantities v_j.

Define

$$u = \frac{\sqrt{\rho_R}u_R + \sqrt{\rho_L}u_L}{\sqrt{\rho_R} + \sqrt{\rho_L}}, \;\; H = \frac{\sqrt{\rho_R}H_R + \sqrt{\rho_L}H_L}{\sqrt{\rho_R} + \sqrt{\rho_L}},$$

and

$$c = \sqrt{(\gamma - 1)(H - \frac{u^2}{2})}.$$

Then

$$A_h = \begin{pmatrix} 0 & 1 & 0 \\ -\frac{\gamma+1}{\gamma}\frac{u^2}{2} & \frac{\gamma+1}{\gamma}u & \frac{\gamma-1}{\gamma} \\ -uH & H & u \end{pmatrix}.$$

The eigenvalues of A_h are u, λ^+ and λ^- where

$$\lambda^{\pm} = \frac{\gamma+1}{2\gamma}u \pm \sqrt{(\frac{\gamma+1}{2\gamma}u)^2 + \frac{c^2 - u^2}{\gamma}}. \tag{21}$$

Note that λ^+ and λ^- have the same sign as $u + c$ and $u - c$, and change sign at the sonic line $u = \pm c$. The corresponding eigenvectors of A_h are the columns of

$$T = \begin{pmatrix} 1 & 1 & 1 \\ u & \lambda^+ & \lambda^- \\ \frac{u^2}{2} & H & H \end{pmatrix}.$$

Also the left eigenvectors of A_h are the rows of

$$T^{-1} = \frac{1}{D}\begin{pmatrix} (\lambda^+ - \lambda^-)H & 0 & (\lambda^+ - \lambda^-) \\ -(uH - \lambda^-\frac{u^2}{2}) & H - \frac{u^2}{2} & -(\lambda^- - u) \\ uH - \lambda^+\frac{u^2}{2} & -(H - \frac{u^2}{2}) & \lambda^+ - u \end{pmatrix},$$

where

$$D = (\lambda^+ - \lambda^-)(H - \frac{u^2}{2}) = (\lambda^+ - \lambda^-)\frac{c^2}{\gamma - 1}.$$

Then

$$A_h = T\Lambda T^{-1},$$

where

$$\Lambda = \begin{pmatrix} u & & \\ & \lambda^+ & \\ & & \lambda^- \end{pmatrix}.$$

The same development can be carried out for multidimensional flows. For convenience the formulas for the general multi-dimensional case are presented in the Appendix.

Using the modified linearization both the characteristic upwind scheme and the CUSP scheme can be reformulated as follows to admit steady solutions with constant H.

5.1 Case 1 Characteristic Upwind Scheme

The diffusion for the characteristic upwind scheme is now defined to be

$$d_{j+\frac{1}{2}} = \frac{1}{2}\left|A_{h_{j+\frac{1}{2}}}\right|(w_{j+1} - wj),$$

in which $|A_h|$ is defined to be

$$|A_h| = T\Lambda T^{-1},$$

where T is the eigenvector matrix of A_h, and

$$|\Lambda| = \begin{pmatrix} |u| & & \\ & |\lambda^+| & \\ & & |\lambda^-| \end{pmatrix}.$$

In order to show that the scheme admits a solution with constant H, split the diffusion into two parts

$$d_{j+\frac{1}{2}} = d^{(1)}_{j+\frac{1}{2}} + d^{(2)}_{j+\frac{1}{2}}$$

where $d^{(1)}_{j+\frac{1}{2}}$ is the contribution from $|u|$, and where $d^{(2)}_{j+\frac{1}{2}}$ is the contribution from $|\lambda^+|$ and $|\lambda^-|$. Then

$$\begin{aligned} d^{(2)}_{j+\frac{1}{2}} &= \begin{pmatrix} 1 & 1 & 1 \\ u & \lambda^+ & \lambda^- \\ \frac{u^2}{2} & H & H \end{pmatrix} \begin{pmatrix} 0 & & \\ & |\lambda^+| & \\ & & |\lambda^-| \end{pmatrix} T^{-1}\Delta w_h \\ &= \begin{pmatrix} 0 & |\lambda^+| & |\lambda^-| \\ 0 & |\lambda^+|\,\lambda^+ & |\lambda^-|\,\lambda^- \\ 0 & |\lambda^+|\,H & |\lambda^-|\,H \end{pmatrix} T^{-1}\Delta w_h, \end{aligned}$$

and the third element of $d^{(2)}_{j+\frac{1}{2}}$ equals the first element multiplied by H. Also

$$\begin{aligned} d^{(1)}_{j+\frac{1}{2}} &= \frac{(\gamma-1)\,|u|}{c^2} \begin{pmatrix} 1 & 1 & 1 \\ u & \lambda^+ & \lambda^- \\ \frac{u^2}{2} & H & H \end{pmatrix} \begin{pmatrix} H\Delta\rho - \Delta(\rho H) \\ 0 \\ 0 \end{pmatrix} \\ &= -\frac{(\gamma-1)\rho\,|u|\,\Delta H}{c^2} \begin{pmatrix} 1 \\ u \\ \frac{u^2}{2} \end{pmatrix} \end{aligned}$$

and this is zero if H is constant. Thus both contributions are consistent with a steady solution in which H is constant. The two variations of the characteristic splitting can conveniently be distinguished as the E and H-characteristic schemes.

The property of admitting steady solutions with constant H is not automatically preserved by higher order constructions. If limiters are used to preserve monotonicity [9], and these introduce comparisons of neighboring slopes of the characteristic variables, then the relationship between the diffusive fluxes for the mass and energy equations will no longer be consistent with constant stagnation enthalpy.

5.2 Case 2 CUSP Scheme

The diffusive flux is now expressed as

$$d_{j+\frac{1}{2}} = \frac{1}{2}\alpha^* c\Delta w_h + \frac{1}{2}\beta\Delta f,$$

where Δ denotes the difference from $j+1$ to j. Again equilibrium at the entrance is established by upwinding, while equilibrium at the exit requires

$$\Delta f + \frac{\alpha^* c}{1+\beta}\Delta w_h = (A_h + \frac{\alpha^* c}{1+\beta}I)\Delta w_h = 0.$$

Therefore, $-\frac{\alpha^* c}{1+\beta}$ must be an eigenvalue of A_h, and in the case $u > 0$, positive diffusion is obtained by taking

$$\alpha^* c = -(1+\beta)\lambda^-.$$

Now the split is redefined as

$$f = uw_h + f_p,$$

where

$$f_p = \begin{pmatrix} 0 \\ p \\ 0 \end{pmatrix}$$

and the diffusive flux can be expressed as

$$d_{j+\frac{1}{2}} = \frac{1}{2}\alpha c \Delta w_h + \frac{1}{2}\beta \bar{w}_h \Delta u + \frac{1}{2}\beta \Delta f_p.$$

Then α and β are defined as before by equations (19) and (20), using the modified eigenvalues $\lambda^{\pm}$ defined equation (21). This splitting corresponds to the Liou-Steffen splitting [12, 20]. The splitting in which the convective terms contain ρE corresponds to the wave particle splitting [14, 2]. As in the case of characteristic splitting, the two variations can conveniently be distinguished as the E-CUSP and H-CUSP schemes.

6 Implementation of limiters

In the case of a scalar conservation law, high resolution schemes which guarantee the preservation of the positivity or monotonicity of the solution can be constructed by limiting the action of higher order or anti-diffusive terms, which might otherwise cause extrema to grow. Typically, these schemes, such as both the symmetric and upstream limited positive (SLIP and USLIP) schemes discussed in the previous paper in this series [9], compare the slope of the solution at nearby mesh intervals. The characteristic upwind scheme essentially applies the same construction to the characteristic variables, so that the solution is subject to controls on the formulation or growth of extrema of these variables. The fluxes appearing in the CUSP scheme have different slopes approaching from either side of the sonic line, and use of limiters which depends on comparisons of the slopes of these fluxes can lead to a loss of smoothness in the solution at the entrance to supersonic zones in the flow.

An alternative formulation which avoids this difficulty, and may be used with either the characteristic upwind or the CUSP scheme, is to form the diffusive flux from left and right states at the cell interface. These are interpolated or extrapolated from nearby data, subject to limiters to preserve monotonicity, in a similar manner to the reconstruction of the solution in Van Leer's MUSCL scheme [11]. Let

$$R(u,v) = 1 - \left| \frac{u-v}{|u|+|v|} \right|^q, \tag{22}$$

where q is a positive power. Then $R(u,v) = 0$ when u and v have opposite sign. Also define

$$L(u,v) = \frac{1}{2}R(u,v)(u+v). \tag{23}$$

Let $w^{(k)}$ denote the kth element of the state vector w. Now define left and right states for each dependent variable separately as

$$\begin{aligned} w_L^{(k)} &= w_j^{(k)} + \frac{1}{2}L(\Delta w_{j+\frac{3}{2}}^{(k)}, \Delta w_{j-\frac{1}{2}}^{(k)}) \\ w_R^{(k)} &= w_{j+1}^{(k)} - \frac{1}{2}L(\Delta w_{j+\frac{3}{2}}^{(k)}, \Delta w_{j-\frac{1}{2}}^{(k)}), \end{aligned}$$

where

$$\Delta w_{j+\frac{1}{2}} = w_{j+1} - w_j.$$

Then

$$w_R^{(k)} - w_L^{(k)} = \Delta w_{j+\frac{1}{2}}^{(k)} - L(\Delta w_{j+\frac{3}{2}}^{(k)}, \Delta w_{j-\frac{1}{2}}^{(k)})$$

and in the case of a scalar equation the SLIP scheme [9] is recovered by making the diffusive flux proportional to this difference. To implement the CUSP scheme the pressures p_L and p_R for the left and right states are determined from w_L and w_R. Then the diffusive flux is calculated by substituting w_L for w_j and w_R for w_{j+1} to give

$$d_{j+\frac{1}{2}} = \frac{1}{2}\alpha^* c(w_R - w_L) + \frac{1}{2}\beta(f(w_R) - f(w_L)).$$

Similarly the characteristic upwind scheme is implemented by calculating $A_{j+\frac{1}{2}}$ from w_R and w_L. In the case of the H-characteristic scheme this also allows the higher order construction to admit solutions with constant stagnation enthalpy, because in this case the slope comparisons for the mass and energy equations are equivalent.

An alternative reconstruction is to set

$$\begin{aligned} w_L^{(k)} &= w_j^{(k)} + R(\Delta w_{j+\frac{3}{2}}^{(k)}, \Delta w_{j-\frac{1}{2}}^{(k)})\Delta w_{j-\frac{1}{2}}^{(k)} \\ w_R^{(k)} &= w_j^{(k)} - R(\Delta w_{j+\frac{3}{2}}^{(k)}, \Delta w_{j-\frac{1}{2}}^{(k)})\Delta w_{j+\frac{3}{2}}^{(k)}. \end{aligned}$$

It has been found that essentially similar results are obtained in numerical calculations of steady flows using the two interpolation formulas.

7 Numerical Results

Extensive numerical tests have been performed with the E and H-characteristic and the E and H-CUSP schemes to verify their properties. Results for one, two and three-dimensional flows are presented in sections 7.1, 7.2 and 7.3. The two-dimensional calculations were performed with the author's FLO82 computer program, which uses a cell-centered finite volume scheme [6, 8]. The three-dimensional calculations were performed with FLO67 [7, 8], using a cell-vertex scheme which was modified to allow perfect cancellation of downstream contributions to the fluxes by the diffusive terms [9].

7.1 One dimensional shock

In order to verify the discrete structure of stationary shocks with the various schemes, calculations were performed for a one dimensional problem with initial data containing left and right states compatible with the Rankine-Hugoniot conditions. An intermediate state consisting of the arithmetic average of the left and right states was introduced at a single cell in the center of the domain. With this intermediate state the system is not in equilibrium, and the time dependent equations were solved to find an equilibrium solution with a stationary shock wave separating the left and right states. Tables 1 through 4 shows the results for a shock wave at Mach 20 for the E-characteristic, H-characteristic, E-CUSP and H-CUSP schemes. In all cases the SLIP construction was used with the limiter defined by equations (22) and (23), and $q = 3$. The tables show the values of ρ, u, H, p, M and the entropy $S = \log \frac{p}{\rho^\gamma} - \log\left(\frac{p_L}{\rho_L^\gamma}\right)$. All four schemes display a perfect one point shock structure. The entropy is zero to 4 decimal places upstream of the shock, and is constant to 4 decimal places downstream of the shock. There is a slight excursion of the entropy at the interior point in the results for the H-characteristic and H-CUSP schemes. Correspondingly there is an excursion in the stagnation enthalpy at the interior point in the results for the E-characteristic and E-CUSP schemes. The tables also verify that the SLIP construction produces solutions which are entirely devoid of oscillations both upstream and downstream of the shock wave. Also it does not spread out the shock structure at all. In figure 1, for example, it can be seen that the limited averages of the slopes $\Delta w_{j+\frac{1}{2}}^{(k)}$ and $\Delta w_{j-\frac{3}{2}}^{(k)}$ are zero because $\Delta w_{j-\frac{3}{2}}^{(k)} = 0$. Similarly the limited averages of the slopes $\Delta w_{j+\frac{3}{2}}^{(k)}$ and $\Delta w_{j-\frac{1}{2}}^{(k)}$ are zero because $\Delta w_{j+\frac{3}{2}}^{(k)} = 0$. Thus the SLIP reconstruction exactly reproduces the first order upwind scheme through the shock wave.

I	ρ	u	H	p	M	s
12	1.0000	23.6643	283.5000	1.0000	20.0000	0.0000
13	1.0000	23.6643	283.5000	1.0000	20.0000	0.0000
14	1.0000	23.6643	283.5000	1.0000	20.0000	0.0000
15	1.0000	23.6643	283.5000	1.0000	20.0000	0.0000
16	1.0000	23.6643	283.5000	1.0000	20.0000	0.0000
17	1.0000	23.6643	283.5000	1.0000	20.0000	0.0000
18	1.0000	23.6643	283.5000	1.0000	20.0000	0.0000
19	1.0000	23.6643	283.5000	1.0000	20.0000	0.0000
20	1.0000	23.6643	283.5000	1.0000	20.0000	0.0000
21	1.0000	23.6643	283.5000	1.0000	20.0000	0.0000
22	4.4232	6.9992	268.9099	308.8882	0.7079	37.5269
23	5.9259	3.9930	283.5064	466.5228	0.3803	37.6369
24	5.9260	3.9930	283.5064	466.5228	0.3803	37.6369
25	5.9260	3.9930	283.5064	466.5228	0.3803	37.6369
26	5.9260	3.9930	283.5064	466.5228	0.3803	37.6369
27	5.9260	3.9930	283.5064	466.5228	0.3803	37.6369
28	5.9260	3.9930	283.5064	466.5228	0.3803	37.6369
29	5.9260	3.9930	283.5064	466.5228	0.3803	37.6369
30	5.9260	3.9930	283.5064	466.5228	0.3803	37.6369
31	5.9260	3.9930	283.5064	466.5228	0.3803	37.6369
32	5.9260	3.9930	283.5064	466.5228	0.3803	37.6369

Table 1: Shock Wave at Mach 20: E-characteristic scheme

I	ρ	u	H	p	M	s
12	1.0000	23.6643	283.5000	1.0000	20.0000	0.0000
13	1.0000	23.6643	283.5000	1.0000	20.0000	0.0000
14	1.0000	23.6643	283.5000	1.0000	20.0000	0.0000
15	1.0000	23.6643	283.5000	1.0000	20.0000	0.0000
16	1.0000	23.6643	283.5000	1.0000	20.0000	0.0000
17	1.0000	23.6643	283.5000	1.0000	20.0000	0.0000
18	1.0000	23.6643	283.5000	1.0000	20.0000	0.0000
19	1.0000	23.6643	283.5000	1.0000	20.0000	0.0000
20	1.0000	23.6643	283.5000	1.0000	20.0000	0.0000
21	1.0000	23.6643	283.5000	1.0000	20.0000	0.0000
22	4.2476	7.1962	283.5073	312.6405	0.7089	40.2710
23	5.9259	3.9930	283.5073	466.5208	0.3803	37.6371
24	5.9260	3.9930	283.5073	466.5208	0.3803	37.6371
25	5.9260	3.9930	283.5073	466.5208	0.3803	37.6371
26	5.9260	3.9930	283.5073	466.5208	0.3803	37.6371
27	5.9260	3.9930	283.5073	466.5208	0.3803	37.6371
28	5.9260	3.9930	283.5073	466.5208	0.3803	37.6371
29	5.9260	3.9930	283.5073	466.5208	0.3803	37.6371
30	5.9260	3.9930	283.5073	466.5208	0.3803	37.6371
31	5.9260	3.9930	283.5074	466.5208	0.3803	37.6371
32	5.9260	3.9930	283.5074	466.5208	0.3803	37.6371

Table 2: Shock Wave at Mach 20: H-characteristic scheme

I	ρ	u	H	p	M	s
12	1.0000	23.6643	283.5000	1.0000	20.0000	0.0000
13	1.0000	23.6643	283.5000	1.0000	20.0000	0.0000
14	1.0000	23.6643	283.5000	1.0000	20.0000	0.0000
15	1.0000	23.6643	283.5000	1.0000	20.0000	0.0000
16	1.0000	23.6643	283.5000	1.0000	20.0000	0.0000
17	1.0000	23.6643	283.5000	1.0000	20.0000	0.0000
18	1.0000	23.6643	283.5000	1.0000	20.0000	0.0000
19	1.0000	23.6643	283.5000	1.0000	20.0000	0.0000
20	1.0000	23.6643	283.5000	1.0000	20.0000	0.0000
21	1.0000	23.6643	283.5000	1.0000	20.0000	0.0000
22	4.4011	7.0503	268.7344	306.6689	0.7138	37.5200
23	5.9259	3.9935	283.4970	466.4894	0.3804	37.6357
24	5.9259	3.9935	283.4970	466.4894	0.3804	37.6357
25	5.9259	3.9935	283.4970	466.4894	0.3804	37.6357
26	5.9259	3.9935	283.4970	466.4894	0.3804	37.6357
27	5.9259	3.9935	283.4970	466.4894	0.3804	37.6357
28	5.9259	3.9935	283.4970	466.4894	0.3804	37.6357
29	5.9259	3.9935	283.4970	466.4894	0.3804	37.6357
30	5.9259	3.9935	283.4970	466.4894	0.3804	37.6357
31	5.9259	3.9935	283.4970	466.4894	0.3804	37.6357
32	5.9259	3.9935	283.4970	466.4894	0.3804	37.6357

Table 3: Shock Wave at Mach 20: E-CUSP scheme

I	ρ	u	H	p	M	s
12	1.0000	23.6643	283.5000	1.0000	20.0000	0.0000
13	1.0000	23.6643	283.5000	1.0000	20.0000	0.0000
14	1.0000	23.6643	283.5000	1.0000	20.0000	0.0000
15	1.0000	23.6643	283.5000	1.0000	20.0000	0.0000
16	1.0000	23.6643	283.5000	1.0000	20.0000	0.0000
17	1.0000	23.6643	283.5000	1.0000	20.0000	0.0000
18	1.0000	23.6643	283.5000	1.0000	20.0000	0.0000
19	1.0000	23.6643	283.5000	1.0000	20.0000	0.0000
20	1.0000	23.6643	283.5000	1.0000	20.0000	0.0000
21	1.0000	23.6643	283.5000	1.0000	20.0000	0.0000
22	4.1924	7.3248	283.4960	307.4467	0.7229	40.3353
23	5.9259	3.9935	283.4960	466.4889	0.3804	37.6355
24	5.9259	3.9935	283.4960	466.4889	0.3804	37.6355
25	5.9259	3.9935	283.4960	466.4889	0.3804	37.6355
26	5.9259	3.9935	283.4960	466.4889	0.3804	37.6355
27	5.9259	3.9935	283.4960	466.4889	0.3804	37.6355
28	5.9259	3.9935	283.4960	466.4889	0.3804	37.6355
29	5.9259	3.9935	283.4960	466.4889	0.3804	37.6355
30	5.9259	3.9935	283.4960	466.4889	0.3804	37.6355
31	5.9259	3.9935	283.4960	466.4889	0.3804	37.6355
32	5.9259	3.9935	283.4960	466.4889	0.3804	37.6355

Table 4: Shock Wave at Mach 20: H-CUSP scheme

It may be noted that the mass, momentum and energy of the initial data are not compatible with the final equilibrium state. According to equation (12) the total mass, momentum and energy must remain constant if the outflow flux f_R remains equal to the inflow flux f_L. Therefore f_R must be allowed to vary according to an appropriate outflow boundary condition to allow the total mass, momentum and energy to be adjusted to values compatible with equilibrium.

7.2 Airfoil calculations

The results of transonic flow calculations using the H-characteristic and H-CUSP schemes are compared in figures (3-9). The E-characteristic and E-CUSP schemes produce results which are very similar to the results of the H-characteristic and H-CUSP schemes, with small deviations in stagnation enthalpy. These are eliminated by the H-characteristic and H-CUSP schemes. The final stagnation enthalpy is exactly constant, in accordance with the theory of Section 6. The limiter defined by equations (22) and (23) was again used with $q = 3$ in both schemes to define left and right states in the manner described in section 6. The H-CUSP scheme was simplified by replacing the Roe averages (2) by arithmetic averages, and using $\lambda^{\pm} = u \pm c$ in the formula (20) for β. It was also found that the term $\bar{w}_h \Delta u$ tends to reduce the rate of convergence to a steady state. Therefore it was attenuated by the factor $\frac{|p_R - p_L|}{(|p_R - p_S| + |p_L - p_S|)}$ where p_S is the pressure at sonic speed, and p_L and p_R are the pressures to the left and right. When the flow crosses the sonic line p_S lies between p_L and p_R, and this factor becomes unity. Thus the full scheme is restored at a shock wave. All the calculations were performed with the five stage modified Runge-Kutta time stepping scheme described in reference [9]. Convergence to a steady state was accelerated by the multigrid also described in reference [9], using W-cycles in which a single time step is performed on each grid level during the descent towards coarser grids. The total amount of work in each W-cycle is about the same as two time steps on the fine grid.

Calculations are presented for two well known airfoils, the RAE 2822 and the NACA 0012. The equations were discretized on meshes with O-topology extending out to a radius of about 100 chords. In each case the calculations were performed on a sequence of successively finer meshes from 40x8 to 320x64 cells, while the multigrid cycles on each of these meshes descended to a coarsest mesh of 10x2 cells. Figure 3 shows the inner parts of the 160x32 meshes for the two airfoils. Figures 4-9 show the final results for each scheme on 320x64 meshes for the RAE 2822 airfoil at Mach .75 and 3° angle of attack, and for the NACA 0012 airfoil at Mach .8 and 1.25° angle of attack, and also at Mach .85 and 1° angle of attack. In each case the convergence history is shown for 100 or 200 cycles, while the pressure distribution is displayed after a sufficient number of cycles for its convergence. In the pressure distributions the pressure coefficient $C_p = \frac{p - p_\infty}{\frac{1}{2}\rho_\infty q_\infty^2}$ is plotted with the negative (suction) pressures upward, so that the upper curve represents the flow over the upper side of a lifting airfoil. The convergence histories show the mean rate of change of the density, and also the total number of supersonic points in the flow, which is almost immediately frozen in these calculations. The pressure distribution of the RAE 2822 airfoil converged in only 25 cycles. Convergence was slower for the NACA 0012 airfoil. In the case of flow at Mach .8 and 1.25° angle of attack, additional cycles were needed to damp out a wave downstream of the weak shock wave on the lower surface. It has been suggested that schemes using flux functions which are not differentiable across the sonic line may be less robust than schemes with smooth fluxes [4]. While the rate of convergence to a steady state is a little slower than those reported in [9] with a CUSP scheme using smooth fluxes, the present calculations continue to exhibit fast and reliable convergence to a steady state. These rates of convergence, particularly in the case of the H-CUSP scheme, are exceptionally fast in comparison with other published results.

As a further check on accuracy the drag coefficient should be zero in subsonic flow, or in shock free transonic flow. Tables 5 and 6 show the computed drag coefficient with the H-characteristic and H-CUSP schemes on a sequence of three meshes for three examples. The first two are subsonic flows over the RAE 2822 and NACA 0012 airfoils at Mach .5 and 3° angle of attack. The third is the flow over the shock free Korn airfoil at its design point of Mach .75 and 0° angle of attack. The computed drag coefficients are slightly lower with the H-CUSP scheme: in all three cases the drag coefficient is calculated to be zero to four digits on a 160x32 mesh.

In aeronautical applications the accurate prediction of drag is particularly important, and an error as large as .0005 is significant since the total drag coefficient of the wing of a transport aircraft (including friction, vortex and shock drag) is in the range of .0150.

Mesh	RAE 2822 Mach .50 α 3°	NACA 0012 Mach .50 α 3°	Korn Airfoil Mach .75 α 0°
40x8	.0099	.0089	.0126
80x16	.0024	.0017	.0026
160x32	.0002	.0002	.0001

Table 5: Drag Coefficient on a sequence of meshes: H-characteristic scheme

Mesh	RAE 2822 Mach .50 α 3°	NACA 0012 Mach .50 α 3°	Korn Airfoil Mach .75 α 0°
40x8	.0062	.0047	.0098
80x16	.0013	.0008	.0017
160x32	.0000	.0000	.0000

Table 6: Drag Coefficient on a sequence of meshes: H-CUSP scheme

7.3 Three-dimensional calculations for a swept wing

As a further test of the performance of the H-CUSP scheme, the flow past the ONERA M6 wing was calculated on a mesh with C-H topology and 192x32x48 = 294912 cells. Figure 10 shows the result at Mach .84 and 3.06° angle of attack. This again verifies the non-oscillatory character of the solution, and the sharp resolution of shock waves. In this case 50 cycles were sufficient for convergence of the pressure distributions.

8 Conclusion

It was shown in the first paper in this series [9] that the concept of local extremum diminishing (LED) schemes provides a convenient framework for the formulation of non-oscillatory shock capturing schemes for compressible flow calculations. In the case of scalar conservation laws the LED property can be secured by corresponding symmetric and upstream limited positive (SLIP and USLIP) schemes.

The different scalar constructions can be combined with alternate numerical fluxes to provide a matrix of schemes for the gas dynamic equations. The property of supporting stationary discrete shocks with a single interior point is shared by the characteristic and CUSP schemes. Each of these schemes can be modified to preserve constant stagnation enthalpy in steady flows, giving four variants, the E and H-characteristic schemes, and the E and H-CUSP schemes. The CUSP schemes are inexpensive. They introduce a minimum amount of numerical diffusion as the Mach number approaches zero. They are therefore also appropriate for viscous flow calculations in which it is important not to contaminate the boundary layer.

The theoretical properties of these schemes are verified by numerical calculations of one-dimensional, two-dimensional and three-dimensional steady flows. References [17] and [18] evaluate the accuracy and efficiency of some of these schemes for the calculation of viscous flows. Further studies are needed to evaluate the performance of the schemes for unsteady flows.

Acknowledgment

This work has benefited from the generous support of ARPA under Grant No. N00014-92-J-1796, AFOSR under Grant No. AFOSR-91-0391, and IBM. The warm hospitality of the Aeronautics and Astronautics Department of Stanford University, and NASA Ames Research Center, provided a very favorable environment for the pursuit of this research while the author was on leave from Princeton University.

References

[1] H. Aiso. Admissibility of difference approximations for scalar conservation laws. *Hiroshima Math. Journal*, 23:15–61, 1993.

[2] N. Balakrishnan and S. M. Deshpande. New upwind schemes with wave-particle splitting for inviscid compressible flows. *Report 91 FM 12*, Indian Institute of Science, 1991.

[3] B. Einfeldt. On Godunov-type methods for gas dynamics. *SIAM J. Num. Anal.*, 25:294–318, 1988.

[4] B. Engquist and Q. Q. Huyuh. Iterative gradient-Newton type methods for steady shock computations. In *Proceedings of the 5th U.S./Mexico Workshop, Advances in Numerical PDESs and Optimization*, SIAM, 1989.

[5] A. Harten, P.D. Lax, and B. Van Leer. On upstream differencing and Godunov-type schemes for hyperbolic conservation laws. *SIAM Review*, 25:35–61, 1983.

[6] A. Jameson. Non-oscillatory shock capturing scheme using flux limited dissipation. In B.E. Engquist, S. Osher, and R.C.J. Sommerville, editors, *Lectures in Applied Mathematics, Vol. 22, Part 1, Large Scale Computations in Fluid Mechanics*, pages 345–370. AMS, 1985.

[7] A. Jameson. A vertex based multigrid algorithm for three-dimensional compressible flow calculations. In T.E. Tezduar and T.J.R. Hughes, editors, *Numerical Methods for Compressible Flow - Finite Difference, Element And Volume Techniques*, 1986. ASME Publication AMD 78.

[8] A. Jameson. Successes and challenges in computational aerodynamics. *AIAA paper 87-1184-CP*, AIAA 8th Computational Fluid Dynamics Conference, Honolulu, Hawaii, 1987.

[9] A. Jameson. Analysis and design of numerical schemes for gas dynamics 1, artificial diffusion, upwind biasing, limiters and their effect on multigrid convergence. *Int. J. of Comp. Fluid Dyn.*, To Appear.

[10] B. Van Leer. Towards the ultimate conservative difference scheme. III upstream-centered finite-difference schemes for ideal compressible flow. *J. Comp. Phys.*, 23:263–275, 1975.

[11] B. Van Leer. Towards the ultimate conservative difference scheme. V a second order sequel to Godunov's method. *J. Comp. Phys.*, 32:101–136, 1979.

[12] M-S. Liou and C.J. Steffen. A new flux splitting scheme. *J. Comp. Phys.*, 107:23–39, 1993.

[13] C. C. Lytton. Solution of the Euler equations for transonic flow over a lifting aerofoil – the Bernoulli formulation (Roe/Lytton method). *J. Comp. Phys.*, 73:395–431, 1987.

[14] S. V. Rao and S. M. Deshpande. A class of efficient kinetic upwind methods for compressible flows. *Report 91 FM 11*, Indian Institute of Science, 1991.

[15] P.L. Roe. Approximate Riemann solvers, parameter vectors, and difference schemes. *J. Comp. Phys.*, 43:357–372, 1981.

[16] P.L. Roe. Fluctuations and signals - a framework for numerical evolution prolems. In K.W. Morton and M.J. Baines, editors, *Proceedings of IMA Conference on Numerical Methods in Fluid Dynamics*, pages 219–257, Reading, 1981.

[17] S. Tatsumi, L. Martinelli, and A. Jameson. Design, implementation, and validation of flux limited schemes for the solution of the compressible Navier-Stokes equations. *AIAA paper 94-0647*, AIAA 32nd Aerospace Sciences Meeting, Reno, Nevada, January 1994.

[18] S. Tatsumi, L. Martinelli, and A. Jameson. A new high resolution scheme for compressible viscous flows with shocks. *AIAA paper* To Appear, AIAA 33nd Aerospace Sciences Meeting, Reno, Nevada, January 1995.

[19] J. P. Veuillot and H. Viviand. Computation of steady inviscid transonic flows using pseudo-unsteady methods. In A. Rizzi and H. Viviand, editors, *Notes on Numerical Fluid Mechanics, Vol. 3*, pages 45–57. Viewveg, 1981.

[20] Y. Wada and M-S. Liou. A flux splitting scheme with high-resolution and robustness for discontinuities. *AIAA paper 94-0083*, AIAA 32nd Aerospace Sciences Meeting, Reno, Nevada, January 1994.

Appendix: Eigenvalues and Eigenvectors for Gas Dynamic Equations

The Euler equations which describe the three-dimensional flow of an inviscid gas can be written as

$$\frac{d}{dt}\int_\Omega W\,dV + \int_{\partial\Omega}(F_x dS_x + F_y dS_y + F_z dS_z) = 0 \tag{24}$$

where W is the state vector, F_x, F_y and F_z are the flux vectors, and dS_x, dS_y and dS_z are the projections of the surface element in the x, y and z coordinate directions. Let u, v and w be the velocity components and ρ, p, E and H the density, pressure, total energy and total enthalpy. Then

$$W = \begin{Bmatrix} \rho \\ \rho u \\ \rho v \\ \rho w \\ \rho E \end{Bmatrix},\ F_x = \begin{Bmatrix} \rho u \\ \rho uu + p \\ \rho uv \\ \rho uw \\ \rho uH \end{Bmatrix},\ F_y = \begin{Bmatrix} \rho v \\ \rho vu \\ \rho vv + p \\ \rho vw \\ \rho vH \end{Bmatrix},\ F_z = \begin{Bmatrix} \rho w \\ \rho wu \\ \rho wv \\ \rho ww + p \\ \rho wH \end{Bmatrix} \tag{25}$$

Also,

$$p = (\gamma - 1)\,\rho\left(E - \frac{q^2}{2}\right),\quad H = E + \frac{p}{\rho} = \frac{c^2}{\gamma - 1} + \frac{q^2}{2} \tag{26}$$

where q is the flow speed, and c is the speed of sound,

$$q^2 = u^2 + v^2 + w^2,\quad c^2 = \frac{\gamma p}{\rho} \tag{27}$$

When flow is smooth it can be represented by the quasi-linear differential equation

$$\frac{\partial W}{\partial t} + A_x\frac{\partial W}{\partial x} + A_y\frac{\partial W}{\partial y} + A_z\frac{\partial W}{\partial z} = 0 \tag{28}$$

where A_x, A_y and A_z are the Jacobian matrices

$$A_x = \frac{\partial F_x}{\partial W},\ A_y = \frac{\partial F_y}{\partial W},\ A_z = \frac{\partial F_z}{\partial W}$$

Under a change of variables to a new state vector $\tilde{W}$, equation (28) is transformed to

$$\frac{\partial \tilde{W}}{\partial t} + \tilde{A}_x\frac{\partial \tilde{W}}{\partial x} + \tilde{A}_y\frac{\partial \tilde{W}}{\partial y} + \tilde{A}_z\frac{\partial \tilde{W}}{\partial z} = 0$$

where

$$A_x = \tilde{M}\tilde{A}_x\tilde{M}^{-1},\quad A_y = \tilde{M}\tilde{A}_y\tilde{M}^{-1},\quad A_z = \tilde{M}\tilde{A}_z\tilde{M}^{-1}$$

and

$$\tilde{M} = \frac{\partial W}{\partial \tilde{W}}$$

The finite volume discretization requires the evaluation of the flux through a face with vector area S,

$$F = F_x S_x + F_y S_y + F_z S_z.$$

The corresponding Jacobian matrix is

$$A = \frac{\partial F}{\partial W} = S_x A_x + S_y A_y + S_z A_z.$$

Let S be the magnitude of the face area

$$S^2 = S_x^2 + S_y^2 + S_z^2$$

and n_x, n_y and n_z be the components of the unit normal

$$n_x = \frac{S_x}{S}, \;\; n_y = \frac{S_y}{S}, \;\; n_z = \frac{S_z}{S}$$

Also let Q be the flux rate

$$Q = uS_x + vS_y + wS_z.$$

Then the Jacobian matrix can be decomposed as

$$A = M\hat{A}M^{-1}$$

where

$$\hat{M} = \begin{pmatrix} 1 & 0 & 0 & 0 & 0 \\ u & 1 & 0 & 0 & 0 \\ v & 0 & 1 & 0 & 0 \\ w & 0 & 0 & 1 & 0 \\ \frac{q^2}{2} & u & v & w & \frac{1}{\gamma-1} \end{pmatrix}, \;\; \hat{M}^{-1} = \begin{pmatrix} 1 & 0 & 0 & 0 & 0 \\ -u & 1 & 0 & 0 & 0 \\ -v & 0 & 1 & 0 & 0 \\ -w & 0 & 0 & 1 & 0 \\ (\gamma-1)\frac{q^2}{2} & -(\gamma-1)u & -(\gamma-1)v & -(\gamma-1)w & \gamma-1 \end{pmatrix}$$

and

$$\hat{A} = \begin{pmatrix} Q & S_x & S_y & S_z & 0 \\ 0 & Q & 0 & 0 & S_x \\ 0 & 0 & Q & 0 & S_y \\ 0 & 0 & 0 & Q & S_z \\ 0 & S_x c^2 & S_y c^2 & S_z c^2 & Q \end{pmatrix}$$

Also the further transformation

$$\hat{A} = DP\bar{A}P^{-1}D^{-1}$$

where

$$D = \begin{pmatrix} 1 & 0 & 0 & 0 & 0 \\ 0 & c & 0 & 0 & 0 \\ 0 & 0 & c & 0 & 0 \\ 0 & 0 & 0 & c & 0 \\ 0 & 0 & 0 & 0 & c^2 \end{pmatrix}, \;\; D^{-1} = \begin{pmatrix} 1 & 0 & 0 & 0 & 0 \\ 0 & \frac{1}{c} & 0 & 0 & 0 \\ 0 & 0 & \frac{1}{c} & 0 & 0 \\ 0 & 0 & 0 & \frac{1}{c} & 0 \\ 0 & 0 & 0 & 0 & \frac{1}{c^2} \end{pmatrix}$$

$$P = \begin{pmatrix} 1 & 0 & 0 & 0 & 1 \\ 0 & 1 & 0 & 0 & 0 \\ 0 & 0 & 1 & 0 & 0 \\ 0 & 0 & 0 & 1 & 0 \\ 1 & 0 & 0 & 0 & 0 \end{pmatrix}, \;\; P^{-1} = \begin{pmatrix} 0 & 0 & 0 & 0 & 1 \\ 0 & 1 & 0 & 0 & 0 \\ 0 & 0 & 1 & 0 & 0 \\ 0 & 0 & 0 & 1 & 0 \\ 1 & 0 & 0 & 0 & -1 \end{pmatrix}$$

produces the symmetric form

$$\bar{A} = \begin{pmatrix} Q & S_x c & S_y c & S_z c & 0 \\ S_x c & Q & 0 & 0 & 0 \\ S_y c & 0 & Q & 0 & 0 \\ S_z c & 0 & 0 & Q & 0 \\ 0 & 0 & 0 & 0 & Q \end{pmatrix}$$

Then $\hat{A}$, $\bar{A}$, and A can be decomposed as

$$\hat{A} = \hat{R}\Lambda\hat{R}^{-1}, \;\; \bar{A} = \bar{R}\Lambda\bar{R}^{-1}, \;\; A = R\Lambda R^{-1}$$

where the diagonal matix Λ contains the eigenvalues

$$\Lambda = \begin{pmatrix} Q & 0 & 0 & 0 & 0 \\ 0 & Q & 0 & 0 & 0 \\ 0 & 0 & Q & 0 & 0 \\ 0 & 0 & 0 & Q+cS & 0 \\ 0 & 0 & 0 & 0 & Q-cS \end{pmatrix}$$

Also the right eigenvectors of $\hat{A}$, $\bar{A}$, and A are the columns of

$$\hat{R} = DN, \;\; \bar{R} = P^{-1}N, \;\; R = \hat{M}DN$$

and the left eigenvectors of $\hat{A}$, $\bar{A}$, and A are the rows of

$$\hat{R}^{-1} = N^{-1}D^{-1}, \;\; \bar{R}^{-1} = N^{-1}P, \;\; R^{-1} = N^{-1}D^{-1}\hat{M}^{-1}$$

where

$$N = \begin{pmatrix} n_x & n_y & n_z & 1 & 1 \\ 0 & -n_z & n_y & n_x & -n_x \\ n_z & 0 & -n_x & n_y & -n_y \\ -n_y & n_x & 0 & n_z & -n_z \\ 0 & 0 & 0 & 1 & 1 \end{pmatrix}, \;\; N^{-1} = \begin{pmatrix} n_x & 0 & n_z & -n_y & -n_x \\ n_y & -n_z & 0 & n_x & -n_y \\ n_z & n_y & -n_x & 0 & -n_z \\ 0 & \frac{n_x}{2} & \frac{n_y}{2} & \frac{n_z}{2} & \frac{1}{2} \\ 0 & -\frac{n_x}{2} & -\frac{n_y}{2} & -\frac{n_z}{2} & \frac{1}{2} \end{pmatrix}$$

The decomposition to $\hat{A}$ corresponds to the introduction of primitive variables, scaled by a diagonal matrix,

$$d\hat{W} = \hat{D}d\tilde{W}, \; \tilde{W} = \begin{pmatrix} \rho \\ u \\ v \\ w \\ p \end{pmatrix}, \; \hat{D} = \begin{pmatrix} 1 & 0 & 0 & 0 & 0 \\ 0 & \rho & 0 & 0 & 0 \\ 0 & 0 & \rho & 0 & 0 \\ 0 & 0 & 0 & \rho & 0 \\ 0 & 0 & 0 & 0 & \rho \end{pmatrix}$$

The decomposition to $\bar{A}$ corresponds to the introduction of symmetrizing variables dW, defined in differential form, scaled by another diagonal matrix

$$d\bar{W} = \bar{D}d\mathcal{W}, \; \mathcal{W} = \begin{pmatrix} \frac{d\rho}{\rho c} \\ du \\ dv \\ dw \\ dp - c^2 d\rho \end{pmatrix}, \; \bar{D} = \begin{pmatrix} \frac{\rho}{c} & 0 & 0 & 0 & 0 \\ 0 & \frac{\rho}{c} & 0 & 0 & 0 \\ 0 & 0 & \frac{\rho}{c} & 0 & 0 \\ 0 & 0 & 0 & \frac{\rho}{c} & 0 \\ 0 & 0 & 0 & 0 & -\frac{1}{c^2} \end{pmatrix}$$

Multiplying out $\hat{M}DN$, the right eigenvectors of A can be expressed as follows. Set

$$v_0 = \begin{pmatrix} 1 \\ u \\ v \\ w \\ \frac{q^2}{2} \end{pmatrix}, \; v_1 = \begin{pmatrix} 0 \\ 0 \\ n_z \\ -n_y \\ vn_z - wn_y \end{pmatrix}, \; v_2 = \begin{pmatrix} 0 \\ -n_y \\ 0 \\ n_x \\ wn_x - vn_z \end{pmatrix}, \; v_3 = \begin{pmatrix} 0 \\ n_y \\ -n_x \\ 0 \\ un_y - vn_x \end{pmatrix}$$

Then the eigenvectors corresponding to the eigenvalue Q are

$$r_1 = n_x v_0 + v_1, \; r_2 = n_y v_0 + v_2, \; r_3 = n_z v_0 + v_3,$$

Here v_0 represents an entropy wave and v_{12} represent vorticity waves. Also let q_n denote the normal velocity Q/S, and set

$$v_4 = \begin{pmatrix} 1 \\ u \\ v \\ w \\ H \end{pmatrix}, \; v_5 = \begin{pmatrix} 0 \\ n_x \\ n_y \\ n_z \\ q_n \end{pmatrix}$$

Then the last two eigenvectors, corresponding to pressure waves, are

$$r_4 = v_4 + cv_5, \; r_5 = v_4 - cv_5,$$

The H-characteristic and H-CUSP schemes introduce the modified Jacobian matrix

$$A_h = \frac{\partial F}{\partial w_h}$$

where w_h is the modified state vector

$$w_h = \begin{pmatrix} \rho \\ \rho u \\ \rho v \\ \rho w \\ \rho H \end{pmatrix}$$

Using transformations of the same kind as those that were used for the standard Jacobian matrix, this can be decomposed as

$$A_h = \hat{M}_h \hat{A}_h \hat{M}_h^{-1}$$

where

$$\hat{M}_h = \begin{pmatrix} 1 & 0 & 0 & 0 & 0 \\ u & 1 & 0 & 0 & 0 \\ v & 0 & 1 & 0 & 0 \\ w & 0 & 0 & 1 & 0 \\ \frac{q^2}{2} & u & v & w & \frac{\gamma}{\gamma-1} \end{pmatrix}, \; \hat{M}_h^{-1} = \begin{pmatrix} 1 & 0 & 0 & 0 & 0 \\ -u & 1 & 0 & 0 & 0 \\ -v & 0 & 1 & 0 & 0 \\ -w & 0 & 0 & 1 & 0 \\ \frac{\gamma-1}{\gamma}\frac{q^2}{2} & -\frac{\gamma-1}{\gamma}u & -\frac{\gamma-1}{\gamma}v & -\frac{\gamma-1}{\gamma}w & \frac{\gamma-1}{\gamma} \end{pmatrix}$$

and

$$\hat{A}_h = \begin{pmatrix} Q & S_x & S_y & S_z & 0 \\ 0 & Q & 0 & 0 & S_x \\ 0 & 0 & Q & 0 & S_y \\ 0 & 0 & 0 & Q & S_z \\ 0 & S_x\frac{c^2}{\gamma} & S_y\frac{c^2}{\gamma} & S_z\frac{c^2}{\gamma} & \frac{Q}{\gamma} \end{pmatrix}$$

Here

$$\hat{M}_h = \hat{M} D_h, \;\; \hat{M}_h^{-1} = D_h^{-1}\hat{M}^{-1}, \;\; \hat{A}_h = D_h^{-1}\hat{A}$$

where

$$D_h = \begin{pmatrix} 1 & 0 & 0 & 0 & 0 \\ 0 & 1 & 0 & 0 & 0 \\ 0 & 0 & 1 & 0 & 0 \\ 0 & 0 & 0 & 1 & 0 \\ 0 & 0 & 0 & 0 & \gamma \end{pmatrix}$$

The eigenvalues of $\hat{A}_h$, and also those of A_h, since they can be derived from $\hat{A}_h$ by a similarity transformation, are Q ,Q ,Q ,λ^+, and λ^- where

$$\lambda^{\pm} \;\; = \;\; \frac{\gamma+1}{2\gamma}Q \pm \sqrt{\left(\frac{\gamma+1}{2\gamma}Q\right)^2 + \frac{c^2S^2 - Q^2}{\gamma}}$$

$$= \frac{\gamma+1}{2\gamma}Q \pm \sqrt{\left(\frac{\gamma-1}{2\gamma}Q\right)^2 + \frac{c^2S^2}{\gamma}}$$

Thus λ^+ and λ^- change sign when $Q = \pm cS$, and λ^+ has the same sign as $Q + cS$, while λ^- has the same sign as $Q - cS$. It is convenient to set

$$\begin{aligned} \sigma &= \frac{\gamma-1}{2\gamma}\frac{Q}{cS}, \qquad \mu = \sqrt{\sigma^2 + \frac{1}{\gamma}} \\ \alpha^+ &= \frac{\lambda^+ - Q}{cS} = \mu - \sigma, \; \alpha^- = \frac{\lambda^- - Q}{cS} = -(\mu + \sigma) \end{aligned}$$

Now $\hat{A}_h$ can be decomposed as

$$\hat{A}_h = \hat{R}_h \Lambda_h \hat{R}_h^{-1}$$

where

$$\Lambda_h = \begin{pmatrix} Q & 0 & 0 & 0 & 0 \\ 0 & Q & 0 & 0 & 0 \\ 0 & 0 & Q & 0 & 0 \\ 0 & 0 & 0 & \lambda^+ & 0 \\ 0 & 0 & 0 & 0 & \lambda^- \end{pmatrix}$$

Also

$$\hat{R}_h = DN_h, \;\; \hat{R}_h^{-1} = N_h^{-1}D^{-1}$$

where D is the same diagonal scaling matrix as before, and

$$N_h = \begin{pmatrix} n_x & n_y & n_z & 1 & 1 \\ 0 & -n_z & n_y & \alpha^+ n_x & \alpha^- n_x \\ n_z & 0 & -n_x & \alpha^+ n_y & \alpha^- n_y \\ -n_y & n_x & 0 & \alpha^+ n_z & \alpha^- n_z \\ 0 & 0 & 0 & {\alpha^+}^2 & {\alpha^-}^2 \end{pmatrix}$$

with the inverse

$$N_h^{-1} = \begin{pmatrix} n_x & -2\gamma\sigma n_x^2 & n_z - 2\gamma\sigma n_y n_x & -n_y - 2\gamma\sigma n_z n_x & \frac{n_x}{\alpha^+\alpha^-} \\ n_y & -n_z - 2\gamma\sigma n_x n_y & -2\gamma\sigma n_y^2 & n_x - 2\gamma\sigma n_z n_y & \frac{n_y}{\alpha^+\alpha^-} \\ n_z & n_y - 2\gamma\sigma n_x n_z & -n_x - 2\gamma\sigma n_y n_z & -2\gamma\sigma n_z^2 & \frac{n_z}{\alpha^+\alpha^-} \\ 0 & \frac{-\alpha^-}{2\mu\alpha^+} n_x & \frac{-\alpha^-}{2\mu\alpha^+} n_y & \frac{-\alpha^-}{2\mu\alpha^+} n_z & \frac{1}{2\mu\alpha^+} \\ 0 & \frac{\alpha^+}{2\mu\alpha^-} n_x & \frac{\alpha^+}{2\mu\alpha^-} n_y & \frac{\alpha^+}{2\mu\alpha^-} n_z & \frac{-1}{2\mu\alpha^-} \end{pmatrix}$$

The formulas for the standard Jacobian matrix are recovered by setting $\alpha^+ = 1$, $\alpha^- = -1$, $\mu = \frac{1}{2}(\alpha^+ - \alpha^-) = 1$, $\sigma = -\frac{1}{2}(\alpha^+ + \alpha^-) = 0$. Correspondingly, A_h can now be represented as

$$A_h = R_h \Lambda_h R_h^{-1}$$

where the right eigenvectors of A_h are the columns of

$$R_h = \hat{M}_h \hat{R}_h = \hat{M}_h D N_h$$

and the left eigenvectors of A_h are the rows of

$$R_h^{-1} = \hat{R}_h^{-1}\hat{M}_h^{-1} = N_h^{-1}D^{-1}\hat{M}_h^{-1}$$

These decompositions of A and A_h express every element in terms of velocities and metric quantities, while the density is completely eliminated from the formulas.

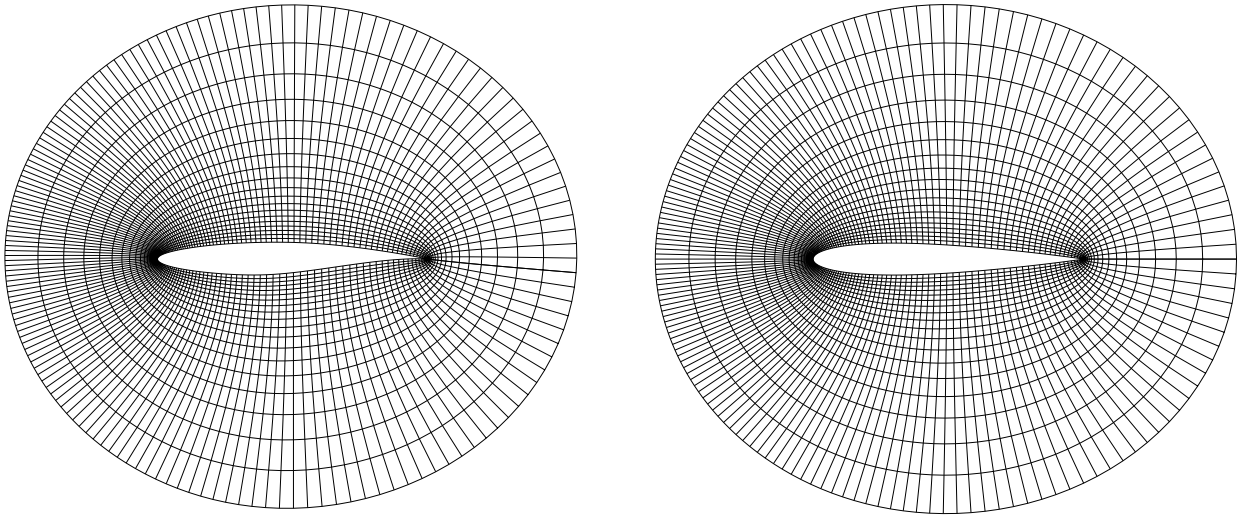

3a: RAE-2822 Airfoil

3b: NACA-0012 Airfoil

Figure 3: O-Topology Meshes, 160x32

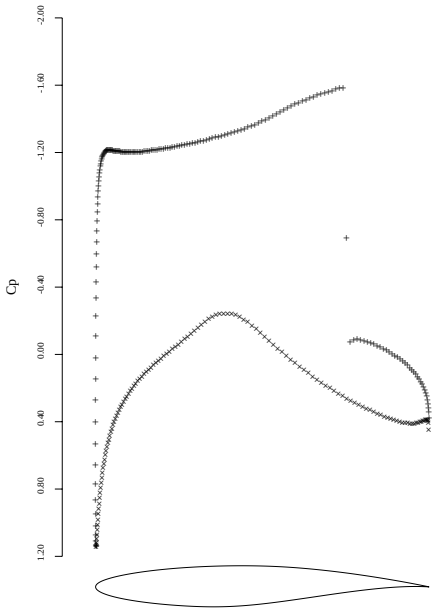

4a: C_p after 25 Cycles.
$C_l = 1.1227$, $C_d = 0.0460$.

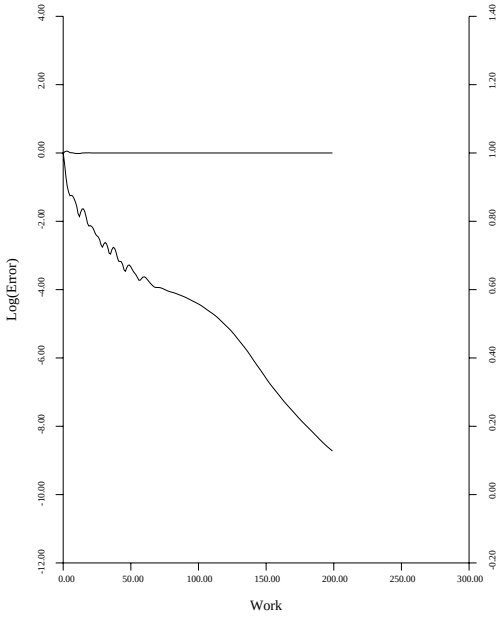

4b: Convergence.

Figure 4: RAE-2822 Airfoil at Mach 0.750 and $\alpha = 3.0°$
H-characteristic Scheme.

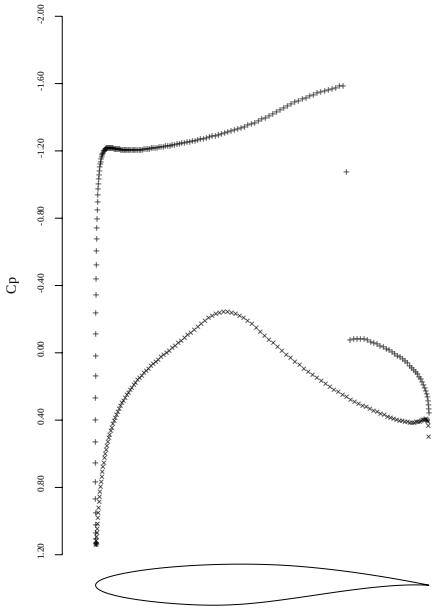

5a: C_p after 25 Cycles.
$C_l = 1.1312$, $C_d = 0.0469$.

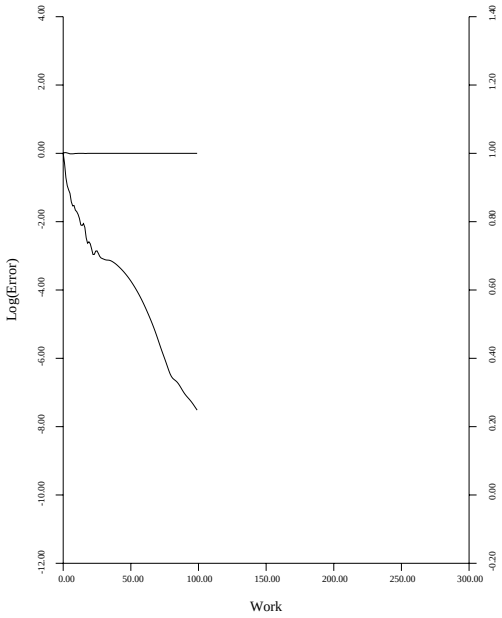

5b: Convergence.

Figure 5: RAE-2822 Airfoil at Mach 0.750 and $\alpha = 3.0°$
H-CUSP Scheme.

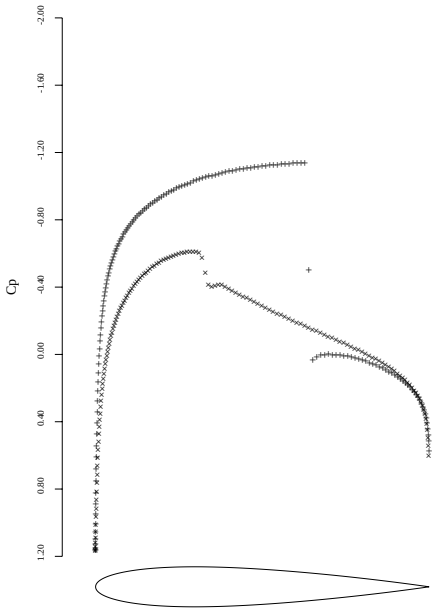

6a: C_p after 75 Cycles.
$C_l = 0.3620$, $C_d = 0.0230$.

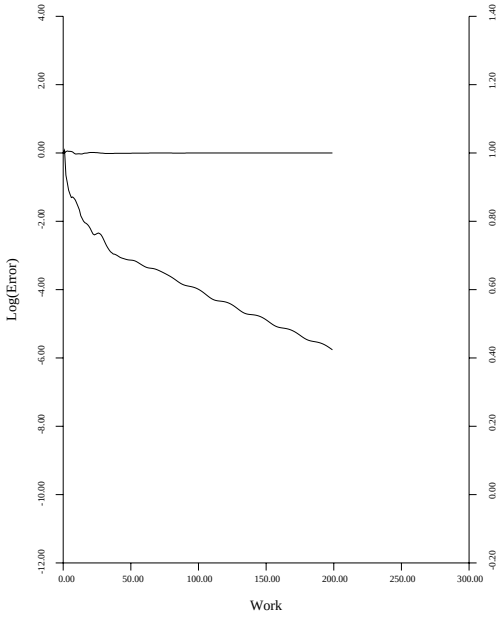

6b: Convergence.

Figure 6: NACA-0012 Airfoil at Mach 0.800 and $\alpha = 1.25°$
H-characteristic Scheme.

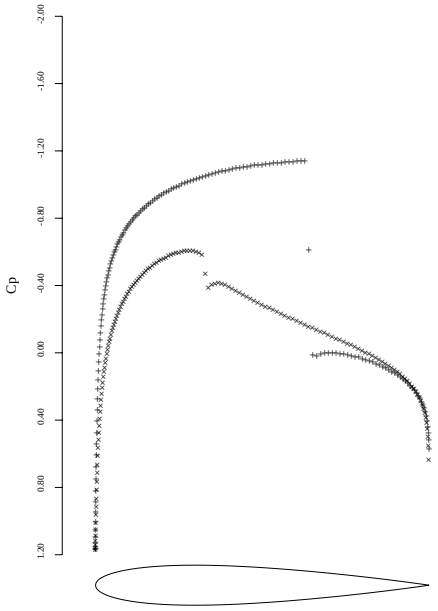

7a: C_p after 35 Cycles.
$C_l = 0.3654$, $C_d = 0.0232$.

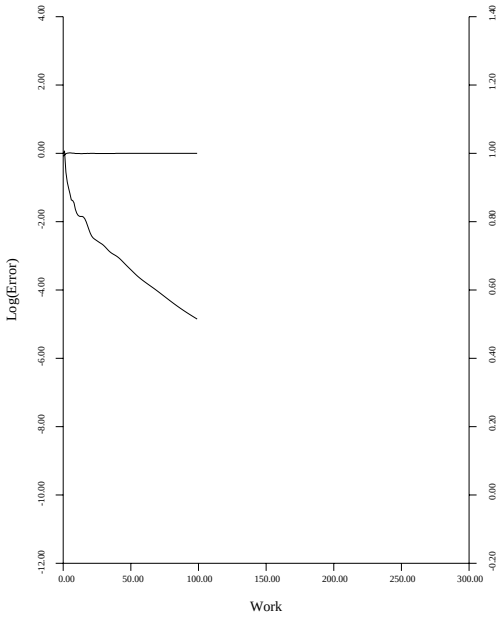

7b: Convergence.

Figure 7: NACA-0012 Airfoil at Mach 0.800 and $\alpha = 1.25°$
H-CUSP Scheme.

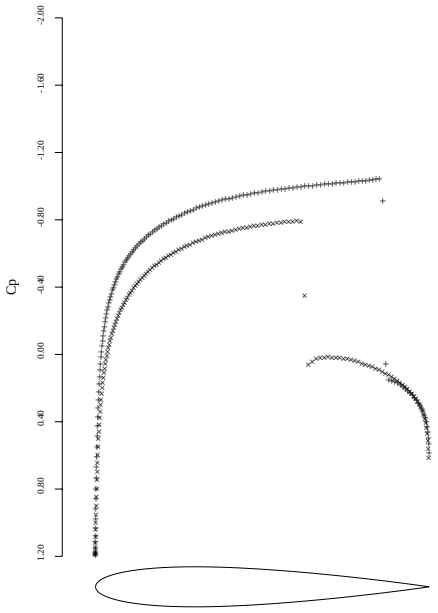

8a: C_p after 75 Cycles.
$C_l = 0.3818$, $C_d = 0.0580$.

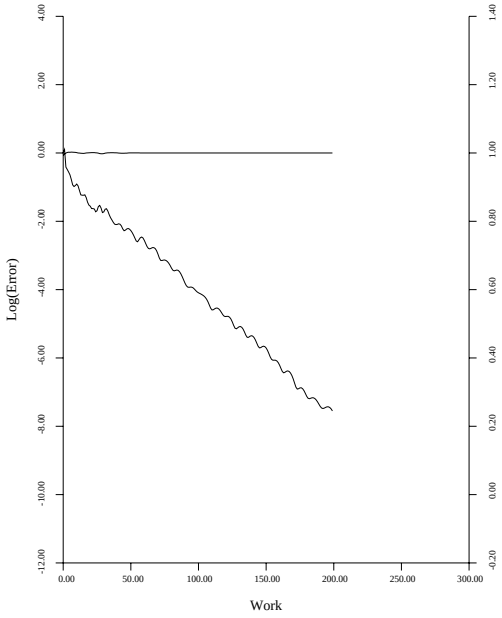

8b: Convergence.

Figure 8: NACA-0012 Airfoil at Mach 0.850 and $\alpha = 1.0°$
H-characteristic Scheme.

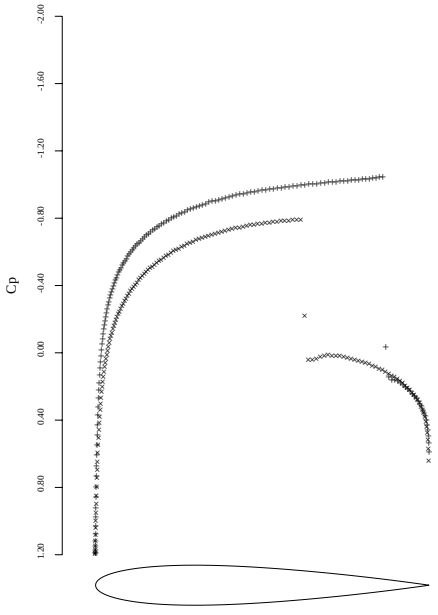

9a: C_p after 35 Cycles.
$C_l = 0.3861$, $C_d = 0.0582$.

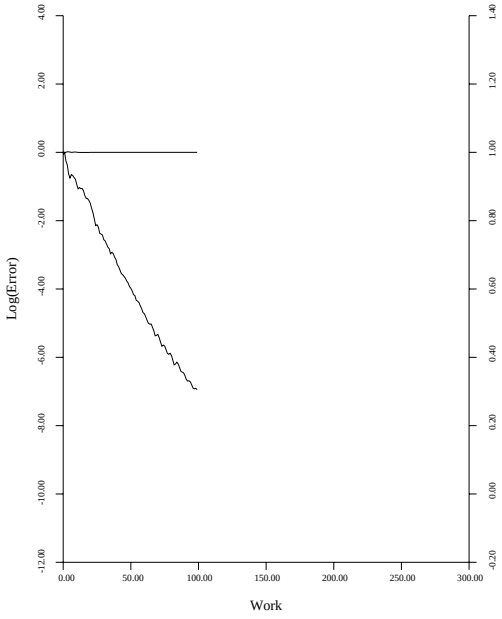

9b: Convergence.

Figure 9: NACA-0012 Airfoil at Mach 0.850 and $\alpha = 1.0°$
H-CUSP Scheme.

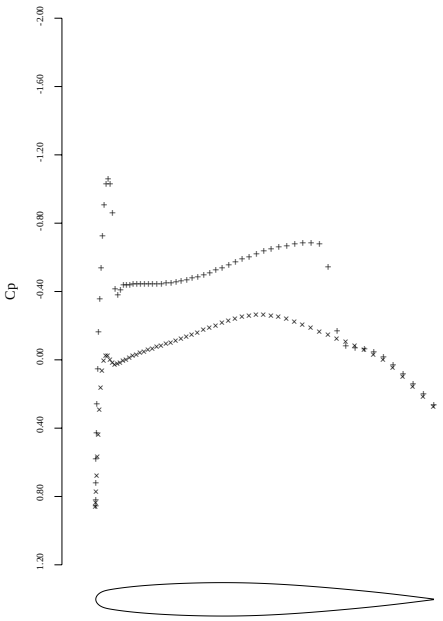

10a: 12.50% Span.
$C_l = 0.2933$, $C_d = 0.0274$.

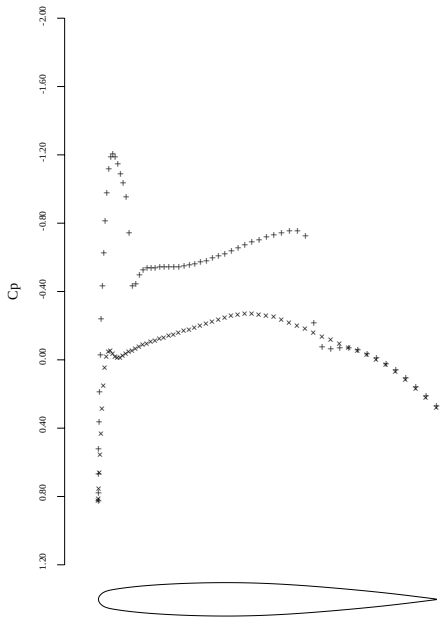

10b: 31.25% Span.
$C_l = 0.3139$, $C_d = 0.0159$.

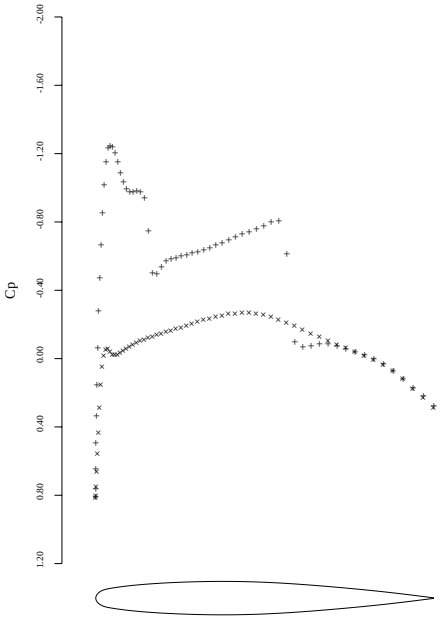

10c: 50.00% Span.
$C_l = 0.3262$, $C_d = 0.0089$.

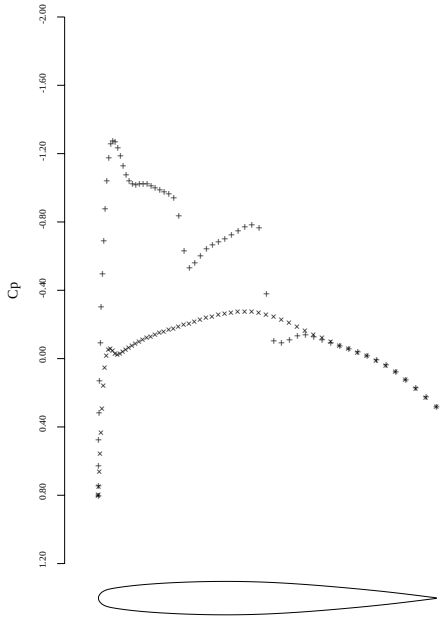

10d: 68.75% Span.
$C_l = 0.3195$, $C_d = 0.0026$.

Figure 10: Onera M6 Wing.
Mach 0.840, Angle of Attack 3.06°, 192×32×48 Mesh.
$C_L = 0.3041$, $C_D = 0.0131$.
H-CUSP scheme.